Meteoritics & Planetary Science 39, Nr 2, 233–246 (2004)
Abstract available online at http://meteoritics.org

Dynamic tensile strength of terrestrial rocks and application to impact cratering

Huirong-Anita AI* and Thomas J. AHRENS

Lindhurst Laboratory of Experimental Geophysics, Seismological Laboratory, California Institute of Technology, Pasadena, California 91125, USA
*Corresponding author. E-mail: ahr@gps.caltech.edu

(Received 7 July 2003; revision accepted 15 January 2004)

Abstract–Dynamic tensile strengths and fracture strengths of 3 terrestrial rocks, San Marcos gabbro, Coconino sandstone, and Sesia eclogite were determined by carrying out flat-plate (PMMA and aluminum) impact experiments on disc-shaped samples in the 5 to 60 m/sec range. Tensile stresses of 125 to 300 MPa and 245 to 580 MPa were induced for gabbro and eclogite, respectively (with duration time of ~1 μs). For sandstone (porosity 25%), tensile stresses normal to bedding of ~13 to 55 MPa were induced (with duration times of 2.4 and ~1.4 μs). Tensile crack failure was detected by the onset of shock-induced (damage) P and S wave velocity reduction.

The dynamic tensile strength of gabbro determined from P and S wave velocity deficits agrees closely with the value of previously determined values by post-impact microscopic examination (~150 MPa). Tensile strength of Coconino sandstone is 20 MPa for a 14 μs duration time and 17 MPa for a 2.4 μs duration time. For Sesia eclogite, the dynamic tensile strength is ~240 MPa. The fracture strength for gabbro is ~250 MPa, ~500 MPa for eclogite, and ~40 MPa for sandstone. Relative crack-induced reduction of S wave velocities is less than that of post-impact P wave velocity reductions for both gabbro and eclogite, indicating that the cracks were predominantly spall cracks.

Impacts upon planetary surfaces induce tensile failure within shock-processed rocks beneath the resulting craters. The depth of cracking beneath impact craters can be determined both by seismic refraction methods for rocks of varying water saturation and, for dry conditions (e.g., the Moon), from gravity anomalies. In principle, depth of cracking is related to the equations-of-state of projectile and target, projectile dimension, and impact velocity. We constructed a crack-depth model applicable to Meteor Crater. For the observed 850 m depth of cracking, our preferred strength scaling model yields an impact velocity of 33 km/s and impactor radius of 9 m for an iron projectile.

INTRODUCTION

The dynamic fracture behavior of rocks plays an important role in fracturing and fragmentation procedures, which vary from industrial processes, such as coal and oil shale fragmentation (Murri et al. 1977), quarrying and mining operations (Carter 1978), in impact or explosive crater formation (O'Keefe and Ahrens 1976), and accretion of planetesimals in the early stages of planetary formation (Matsui and Mizutani 1977).

Dynamic tensile strength experiments on rocks have been carried out by Grady and Hollenbach (1979), Cohn and Ahrens (1981), Lange et al. (1984), Ahrens and Rubin (1993), and others. Previously, three quantitative methods have been used to determine the dynamic tensile strength. These are: 1) the free-surface velocity pullback signal method (Grady and Hollenbach 1979); 2) terminal examination (Cohn and Ahrens 1981; Lange et al. 1984); and 3) ultrasonic post-impact examination (Ahrens and Rubin 1993). The free-surface velocity pullback signal method measures the drop in the target's free-surface velocity upon arrival of the compression wave generated by an expanding tensile crack to determine tensile strength. Method 2 involves microscopic examination of polished thin section samples made from the recovered samples to determine the incipient spall cracks produced by impact. The stress above which microscopically observable cracks appear is assumed to be the dynamic tensile strength. Post-impact ultrasonic examination measures the pre- and post-shot ultrasonic velocities of the samples and relates the shock-induced damage in rocks to shock-induced one-dimensional tensile stresses. The tensile strengths determined by the free-surface velocity pullback signal method and the terminal examination depends crucially on the properties along the narrow zone of tensile failure where

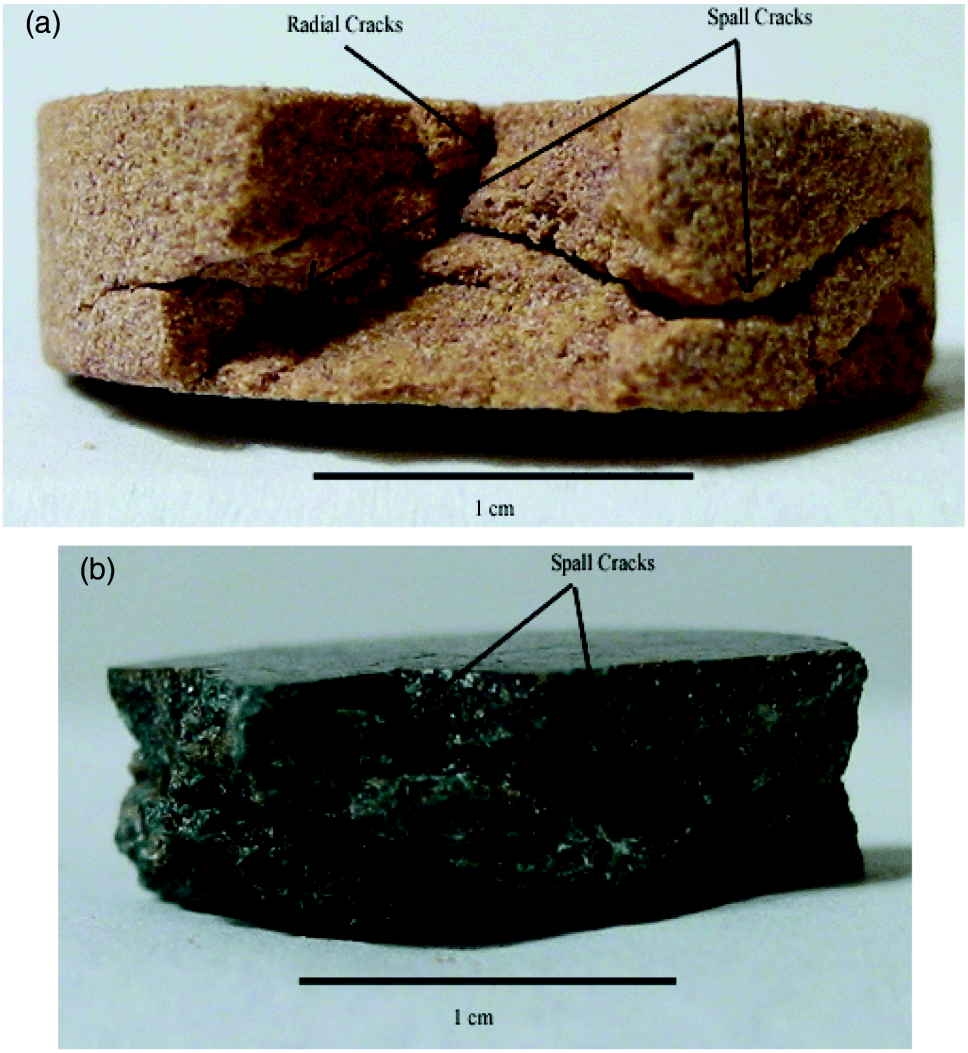

Fig. 1. Recovered samples: a) CS 27; and b) one fragment of SE 5 to show the radial and spall (subhorizonal) cracks observed. The measured velocity reduction of (a) was ~36% and ~40% for P and S wave velocities. The velocity reduction for (b) was unmeasurable.

the rock fractures. Moreover, we note that the sample-cutting process required to examine recovered samples in method 2 could produce additional damage. The ultrasonic method is a superior method, and it is a volume measurement. This method measures crack density instead of the properties of a single crack. For this reason, ultrasonic method 3 is chosen to determine the tensile strength in this work.

Quantitative data on the tensile behavior of many types of rocks and their dependence on strain rate are still lacking. In this study, we selected one igneous rock (San Marcos gabbro), one sedimentary rock (Coconino sandstone), and one metamorphic rock (Sesia eclogite) for determination of the dynamic tensile strength using method 3 above.

SIGNIFICANCE AND LITHOLOGIES OF ROCKS

San Marcos gabbro from Escondido, a well-studied rock (Lange et al. 1984; Ahrens and Rubin 1993; Xia and Ahrens 2001), is chosen for comparison with previous studies. Lange et al. (1984) reported that the density of this rock is 2.867 g/cm^3, the compressional wave velocity (V_p) is 6.36 ± 0.16 km/s, and it has very low initial crack density. The mineral composition of San Marcos gabbro is 67.9% plagioclase, 22.5% amphibole, 2.6% pyroxene, 1.4% quartz, and some trace elements (Lange et al. 1984).

The dynamic tensile strength of Coconino sandstone from Meteor Crater, Arizona is of interest, as Coconino sandstone is one of the main sedimentary rock types of the crater (Shoemaker 1963). The subsurface strata of Meteor Crater have been studied in a refraction survey (Ackermann et al. 1975). Roddy et al (1980) simulated the formation of this crater. However, previously, only dynamic compressive experiments at different strain rates were performed by Ahrens and Gregson (1964) and Shipman et al. (1971) on this type of rock. The block from which the samples are made is yellowish-gray or cream colored and contains sub-parallel

laminae that are separated by thin laminae containing more than average amounts of silt and clay sized grains. Cross-bedding can be seen clearly on the cutting surfaces. Coconino sandstone is composed of 97% quartz and 3% feldspar, with traces of clay and heavy minerals (Ahrens and Gregson 1964). The average grain size is in the range of 0.12–0.15 mm, and the porosity is 24–25% (Ahrens and Gregson 1964; Shipman et al. 1971). The bulk density of our samples was 2.08 ± 0.03 g/cm^3, slightly higher than that reported by Ahrens and Gregson (1964) and Shipman et al. (1971) of 1.99 g/cm^3. Impact and ultrasonic wave measurements are all normal to the bedding of the sandstone.

Eclogite is chosen because it may represent the upper limit of dynamic tensile strength available for terrestrial rocks. The eclogite from the Sesia zone of the Austroalpine system in Italy is metamorphic. Thin section analysis of the rock sample shows that it contains 40% garnet, 45% clinopyroxene, 4% mica, and trace feldspar and opaques. The grain size is 1 to ~1.5 mm, and the bulk density is 3.44 ± 0.04 g/cm^3.

The physical properties of the three types of rocks are listed in Table 1.

EXPERIMENTAL TECHNIQUES

The dynamic tensile strengths of the San Marcos gabbro, Coconino sandstone, and Sesia eclogite were determined by planar impact experiments using a 40 mm compressed gas gun, similar to that described in Cohn and Ahrens (1981). A Lexan projectile carrying a polymethyl methacrylate (PMMA) or aluminum (Al) flyer plate at its front is accelerated by the expansion of precompressed air to velocities in the 5 to 60 m/s range. The initial impact produces compressional shock waves propagating forward into the target and back into the flyer plate. These compressional waves then reflect back as relief waves from the free surfaces of the target and the flyer plate. Tension is produced when the two relief waves meet within the sample. We assume that the magnitude of the tensile stress is equal to that of the original compressive stress, and the initial compressive pulse produced no detectable damage. When the peak tensile stress exceeds the dynamic tensile strength of the rock, cracks start to occur within the sample.

Table 1. Physical properties of experimental materials.[a]

Material	Average ρ, g/cm^3	C_p, km/s	C_s, km/s
San Marcos gabbro	2.867 (2)	6.65 (1) 6.36 (2)	3.57 (1)
Coconino sandstone (velocity normal to bedding)	2.08 (1) 1.99 (3)	2.81 (1)	1.82 (1)
Sesia ecologite	3.44 (1)	6.40 (1)	3.78 (1)
PMMA	1.2	2.8	
Aluminum 2024	2.78	6.36	

[a]Sources: (1) This study; (2) Lange et al. 1984; (3) Ahrens and Gregson 1964.

The choice of PMMA or Al flyer plates depends on the impedances of the rock, defined as the product of the density, ρ, and the compressional velocity, V_p. Al flyer plates are used for San Marcos Gabbro and Sesia Eclogite, with impact velocities of 13 to 30 m/sec, and 24 to 60 m/sec, respectively. PMMA flyer plates are used for Coconino sandstone, with impact velocities of 5 to 22 m/sec. The impact velocities are controlled by varying the pressure of the compressed air. Different impact velocities result in different amplitude tensile stresses. The impact velocity is measured in air by the sequential interruption of three laser beams. The impacted target flies free into a recovery tank, where loose rags prevent further damage.

The targets are shaped as discs with diameters of 22 to 23 mm and thickness of 6.5 to 7 mm. Front and rear surfaces are polished. The achieved parallelism of the sample surfaces was ±0.003 mm for San Marcos gabbro and Sesia eclogite. Surface parallelism ensures that the strain in the ~1 cm central region of the sample is approximated by a one-dimensional strain condition. Less parallelism, ±0.03 mm, was achieved for Coconino Sandstone due to its high porosity. This partially explains the relatively large data scatter of ultrasonic measurements for sandstone. Samples of San Marcos gabbro and Sesia eclogite are cut wet and vacuum-dried for 24 hr before the experiments, while samples of Cononino sandstone are cut dry, to avoid changes in the physical properties of the sample.

In our experiments, the impedance of the flyer plate is less than that of the target, resulting in the separation of target and flyer plate (Ahrens and Rubin 1993). The tensile stress (σ) within the target is given by the acoustic formula (Cohn and Ahrens 1981):

$$\sigma = U_p \frac{\rho_t V_{pt} \rho_i V_{pi}}{\rho_i V_{pi} + \rho_t V_{pt}} \quad (1)$$

where U_p is the projectile velocity, V_p is the compressional seismic velocity, ρ is density, and the subscripts i and t refer to the projectile and target, respectively. The individual density of each sample is used for stress calculation.

The duration time (t_d) of the shock can be approximated by:

$$t_d = \frac{2d_i}{V_{pi}} \quad (2)$$

where d_i is the thickness of the flyer plate.

Pre-shot and post-shot ultrasonic P and S wave velocities were measured for the targets using the ultrasonic pulse transmission method. The reduction of the velocity gives a measure of degradation of the modulus of a micro-cracked body. The P wave transducers are Model V103, Panametrics; the S wave transducers are Model V153, Panametrics. The frequency of transducers used for both wave measurements is 1 MHz. The minimum crack size that the P wave transducers can detect is about one half of the wavelengths of the ultrasonic waves in the media (Heinrich 1991). That is, ~2 mm for San Marcos gabbro and Sesia eclogite and ~1 mm

for Coconino sandstone. A Caltech-made high-voltage pulser with a rise time of about 10 μs is used as a transducer driver. A digital oscilloscope (Gould 4074) is used to record the ultrasonic signals. Panametrics couplant D-12 is used for P wave measurements, and Panametrics couplant SWC is used for S wave measurements. Alcohol and water were used as P and S wave couplant removers, respectively. Aluminum foil (thickness of 0.03 mm) is placed between the sample and the transducers to prevent the samples from being contaminated by the couplants and couplant removers. All the impacts were performed at room temperature and atmospheric pressure.

We define the dynamic tensile strength of the rock as the peak stress above which tensile cracks are observed from a decrease in P or S wave velocities, and the fracture strength is the peak stress above which complete fragmentation happens. According to Ahrens and Rubin (1993), a 2% reduction in P wave velocity, or 3% increase in the radii of the largest cracks present, which corresponds to an increase in crack density of 0.016, is the minimum that could be detected by the ultrasonic method. Here, crack density is expressed as:

$$\varepsilon = N\langle a^3 \rangle \tag{3}$$

where N is the number of cracks per unit volume, and $\langle a^3 \rangle$ is the average of the cube of the crack radii (O'Connell and Budiansky 1974).

RESULTS AND DISCUSSION

Both pre-shot and post-shot ultrasonic compressional and shear wave velocities in the direction perpendicular to the impact surface and V_p/V_s are listed in Table 2, as well as impact velocities and relative tensile stresses for our experiments. Figs. 2 to 4 show velocity reductions with tensile stresses for the 3 types of rocks and Fig. 5 is the V_p/V_s ratio versus tensile stresses. Several important effects are identified below:

1. P and S wave velocity reductions occur with increasing tensile stress for the 3 types of rocks studied (Figs. 2– 4). The highest P wave velocity reduction measured is ~25% for San Marcos gabbro and 10% for S wave velocity (Fig. 2). For Sesia eclogite measurements, the results are 48% and 35% for P and S wave reduction, respectively (Fig. 3). In the Coconino sandstone experiment with 2.4 μs duration time, 30% and 25% are obtained for P and S wave reduction, respectively, which increase to 36% and 40% for the 1.4 μs duration time case (Figs. 4a and 4b).
2. Fig. 2 suggests that the onset of tensile failure of San Marcos gabbro determined by the detectable ultrasonic velocity reduction is between 120 and 150 MPa. This result is comparable with a previous microscopic examination of recovered samples (Lange et al. 1984). Within this range, Lange et al. (1984) reported that

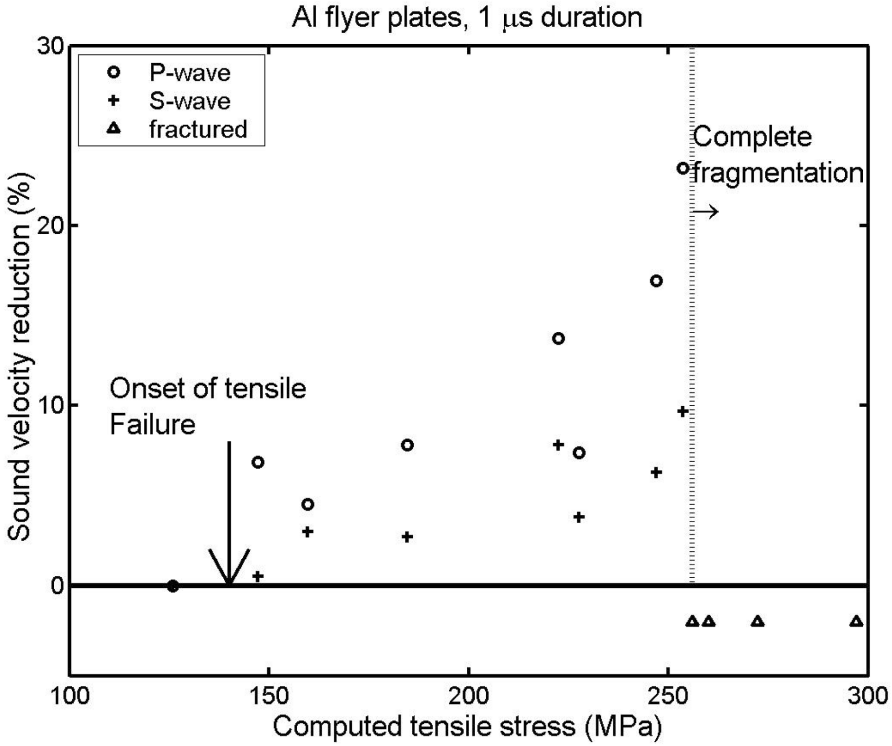

Fig. 2. Velociy measurements for the San Marcos gabbro experiments. The dashed line indicates the pressure above which complete fragmentation occurred.

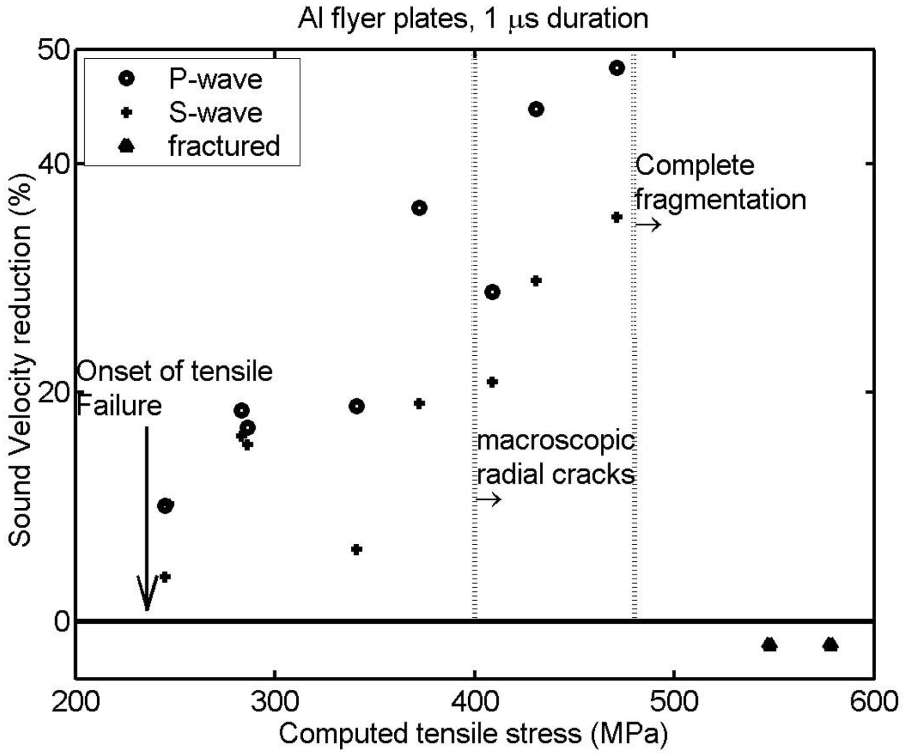

Fig. 3. Velocity measurements for Sesia eclogite measurements. The dashed lines indicate the pressures above which macroscopic radial and complete fragmentation occurred.

incipient cracks, more or less continuous, were observed. Complete fragmentation occurs above 250 MPa. This is determined to be the fracture strength.

3. The onset of tensile failure for Sesia eclogite is ~240 MPa. This is the highest known limit of tensile strength measured by experiment for terrestrial rocks. The observable continuous cracks for Sesia eclogite appear around tensile stress about 400 MPa (Fig. 3). Complete fragmentation occurs above ~500 MPa.
4. The onset of tensile failure for Coconino sandstone, determined from detectable ultrasonic velocity reduction, are ~17 MPa for the 2.4 μs shock duration time and ~20 MPa for the 1.4 μs duration time. Macroscopic radial cracks appear at ~30 MPa and complete fragmentation at ~40 MPa for both cases (Fig. 4).
5. The reduction of P wave velocity is greater than the reduction of S wave velocity for both San Marcos gabbro (Fig. 2) and Sesia eclogite (Fig. 3). There is no obvious relation between P and S wave reduction for Coconino sandstone.
6. All pre-shot and post-shot V_p/V_s values of the 3 types of rocks are shown in Fig. 5. V_p/V_s for pre-shot San Marcos gabbro is 1.9 ± 0.05. For pre-shot Sesia eclogite, V_p/V_s is 1.7 ± 0.13, compatible with the value of Healdsburg eclogite, California (1.74) (Birch 1960) and that of Sunnmoure eclogite, Norway (1.66) (McQueen et al. 1967). For Coconino sandstone, it is 1.5 ± 0.08. The measurable post-shot V_p/V_s value for both San Marcos gabbro and Sesia eclogite is less than the pre-shot value (Figs. 5a and 5b). The post-shot values of both types of rocks decrease with tensile stress, and the difference between pre- and post-shot measurements of V_p/V_s increases with tensile stress. No obvious decrease with computed tensile stress of post-shot V_p/V_s for Coconino sandstone is observed.

Reduction of Velocity by Cracks

The presence of cracks within a rock has long been recognized to decrease the elastic moduli (Birch 1960). O'Connell and Budiansky (1974) developed a theory to calculate the effective bulk modulus ($\overline{K}$), shear modulus ($\overline{G}$), and Poisson ratio ($\overline{\upsilon}$) for a body with a random distribution of cracks:

$$\frac{\overline{K}}{K} = 1 - \frac{16}{9}\left(\frac{1-\overline{\upsilon}^2}{1-2\upsilon}\right)\varepsilon \tag{4}$$

$$\frac{\overline{G}}{G} = 1 - \frac{32}{45}\frac{(1-\overline{\upsilon})(5-\overline{\upsilon})}{(2-\overline{\upsilon})}\varepsilon \tag{5}$$

$$\overline{\upsilon} = \upsilon\left(1 - \frac{16}{9}\varepsilon\right) \tag{6}$$

Table 2. One-dimensional tensile strain impact parameters and pre-shot and post-shot ultrasonic compressional and shear velocities.

Shot[a]	Sample[b]	Flyer plate	Projecile velocity m/s	Tensile stress MPa	Pre-shot V_p, km/s	Pre-shot V_s, km/s	Pre-shot V_p/V_s	Post-shot V_p, km/s	Post-shot V_s, km/s	Post-shot V_p/V_s
G23	SMG#21	Al	15.62	147.27	6.908	3.538	1.95	6.434	3.519	1.83
G24	SMG#22	Al	16.97	159.61	6.833	3.647	1.87	6.524	3.538	1.84
G26	SMG#25	Al	25.19	227.69	6.533	3.479	1.88	6.05	3.347	1.81
G28	SMG#28	Al	27.89	253.66	6.427	3.496	1.84	4.936	3.156	1.56
G29	SMG#29	Al	28.53	272.43	7.137	4.683	1.52	fragmented		
G30	SMG#30	Al	23.78	222.58	6.84	3.618	1.89	5.9	3.337	1.77
G31	SMG#31	Al	32.11	297.15	6.687	3.506	1.91	fragmented		
G32	SMG#32	Al	26.61	247.07	6.727	3.609	1.86	5.588	3.38	1.65
G33	SMG#33	Al	28.51	260	6.461	3.684	1.75	fragmented		
G34	SMG#34	Al	20.1	184.7	6.526	3.474	1.88	6.017	3.379	1.78
G35	SMG#24	Al	13.74	125.89	6.483	3.509	1.85	6.483	3.509	1.85
CS8	CS#10	PMMA	22.068	45.26	2.819	1.807	1.56	fragmented		
CS9	CS#11	PMMA	21.176	44.05	2.937	1.844	1.59	fragmented		
CS10	CS#12	PMMA	20.087	40.94	2.748	1.921	1.43	fragmented		
CS11	CS#13	PMMA	16.63	34.54	2.864	1.88	1.52	1.998	1.299	1.54
CS12	CS#14	PMMA	18.63	38.99	2.934	1.906	1.54	1.99	1.476	1.35
CS13	CS#15	PMMA	15.33	31.32	2.77	1.831	1.51	2.084	1.482	1.41
CS14	CS#16	PMMA	13.72	28.08	2.74	1.735	1.58	2.593	1.51	1.72
CS15	CS#17	PMMA	11.5	23.69	2.795	1.729	1.62	2.594	1.515	1.71
CS16	CS#18	PMMA	8.704	17.84	2.771	1.764	1.57	2.74	1.722	1.59
CS17	CS#19	PMMA	6.413	13.19	2.8	1.777	1.58	2.8	1.777	1.58
CS18	CS#20	PMMA	19.28	39.93	2.809	1.86	1.51	fragmented		
CS19	CS#21	PMMA	14.923	30.55	2.78	1.783	1.56	1.841	1.23	1.5
CS20	CS#22	PMMA	18.476	38.6	2.907	1.873	1.55	fragmented		
CS21	CS#23	PMMA	11.828	23.9	2.703	1.769	1.53	2.38	1.585	1.5
CS22	CS#24	PMMA	7.688	15.84	2.813	1.807	1.56	2.813	1.576	1.78
CS23	CS#25	PMMA	9.984	20.34	2.744	1.693	1.62	2.644	1.535	1.72
CS24	CS#26	PMMA	13.729	28.32	2.831	1.88	1.51	2.359	1.523	1.55
CS25	CS#27	PMMA	16.357	33.76	2.838	1.832	1.55	2.189	1.35	1.62
CS26	CS#28	PMMA	16	32.8	2.766	1.796	1.54	2.023	1.352	1.5
CS27	CS#29	PMMA	16.709	34.67	2.855	1.845	1.55	1.826	1.11	1.65
CS28	CS#30	PMMA	15.075	30.98	2.768	1.877	1.47	2.206	1.443	1.53
SE1	SE#1	Al	60.077	578.12	6.096	3.81	1.6	fragmented		
SE2	SE#2	Al	48.93	471.34	6.083	3.883	1.57	3.139	2.51	1.25
SE3	SE#3	Al	42.21	408.76	6.165	3.909	1.58	4.391	3.09	1.42
SE4	SE#4	Al	33.226	340.7	7.008	3.976	1.76	5.69	3.725	1.53
SE5	SE#5	Al	55.771	547.56	6.329	3.836	1.65	fragmented		
SE6	SE#6	Al	24.1	244.86	6.99	3.888	1.8	6.284	3.736	1.68
SE7	SE#7	Al	38.068	372.15	6.486	3.884	1.67	4.143	3.144	1.32
SE8	SE#9	Al	28.396	283.16	6.574	3.6	1.83	5.361	3.017	1.78
SE9	SE#10	Al	45.92	430.55	5.855	3.389	1.73	3.231	2.38	1.36
SE10	SE#11	A1	30.138	286.37	6.047	3.45	1.75	50.23	2.917	1.72
SE11	SE#8	A1	24.79	246.86	6.771	3.934	1.72	–	3.53	–

[a]Duration for shot G23 to G35 is ~1 μs; duration time for shot CS8 to CS17 is ~2.4 μs; duration time for shot CS18 to CS28 is ~1.4 μs; duration time for shot SE1 to SE11 is ~1 μs.

[b]SMG: San Marcos gabbro; CS: Coconino sandstone; SE: Sesia eclogite.

where K is bulk modulus, G is shear modulus, υ is Poisson ratio of the undamaged body, and ε is crack density. From the equations above, a crack density of 0.05 would produce ~4% P wave reduction and ~1.5% S wave reduction.

For a cracked body, reduction of both P and S wave velocities increase with crack density. This is consistent with our experimental results for all 3 types of rocks (Figs. 2–4). However, the degree of velocity decrease depends on the orientation of cracks. According to theory of O'Connell and Budiansky (1974), reduction of S wave velocity is only

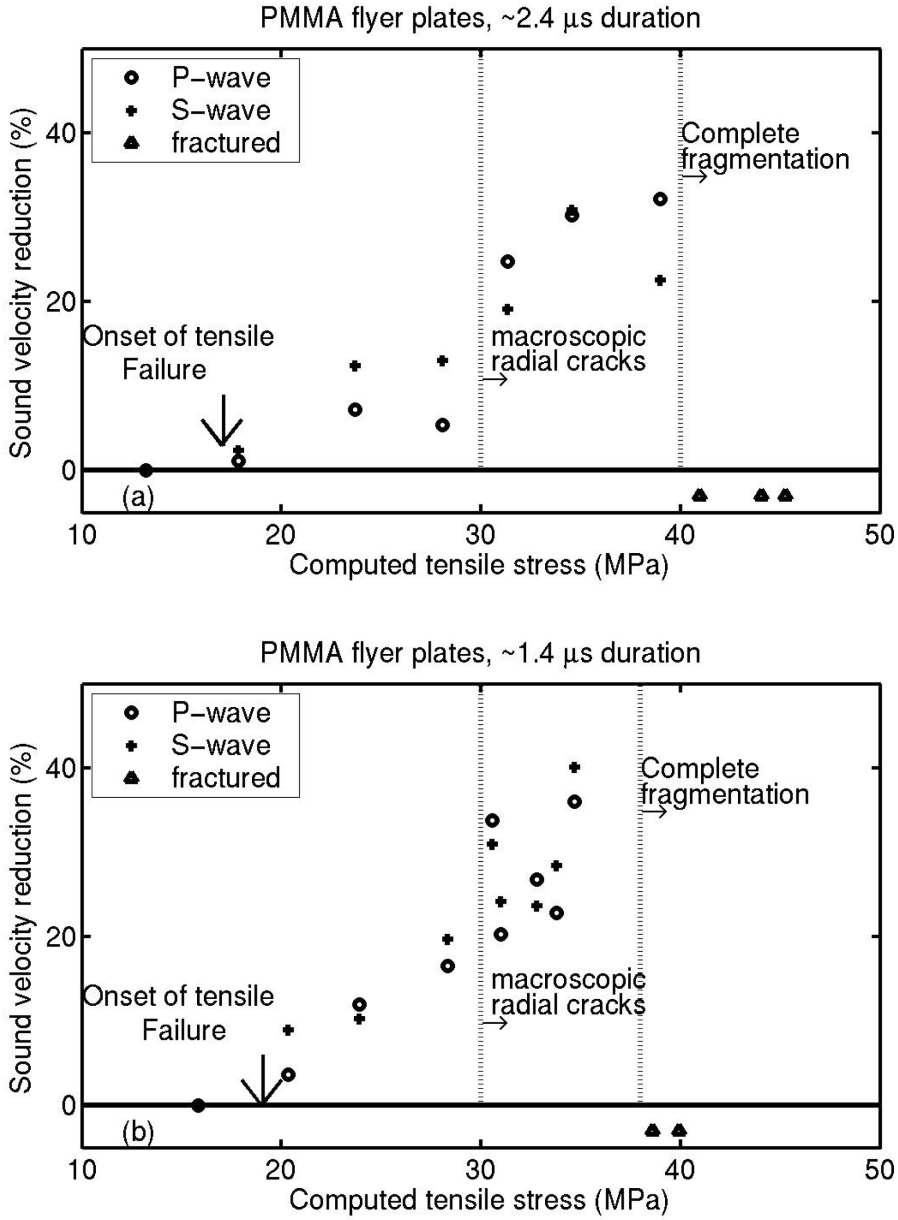

Fig. 4. Velocity measurements of Coconino sandstone for experiments of duration time of (a) 2.4 μs and (b) 1.4 μs. The dashed lines indicate the same as those in Fig. 3.

slightly less than that of P wave velocity for dry rock samples with randomly oriented cracks. For example, a 20% reduction in P wave velocity should be associated with 18% reduction in S wave velocity. If the cracks had a preferential orientation, they would reduce the P wave velocity measured in the direction perpendicular to the crack orientation surface much more than the S wave velocity measured in the same direction. This result has been demonstrated both theoretically (Anderson et al. 1974; Nishizawa 1982) and experimentally (King 2002). According to the calculation of Anderson et al. (1974), for reasonable crack aspect ratios (0.05), a 20% reduction in P wave velocity is associated only with ~5 to ~7% reduction in S wave velocity.

Interaction of release waves emanating from lateral boundaries and planar-impacted surfaces induce both radial and spall cracks in our experiments. Radial cracks are also observed in similar experiments for Bedford limestone by Ahrens and Rubin (1993). These are generated in non-planar deformation of the sample. We believe a major contribution to the loss of one-dimensional symmetry is rarefaction waves reflected from the edges of the sample. These waves propagate into the region of interest producing tensile stresses that are perpendicular to the direction of the impact. Therefore, the strain state inside the sample is not strictly uniaxial. Both radial and face-parallel cracks are expected to contribute to the wave velocity reduction. For San Marcos

gabbro and Sesia eclogite, reduction in P wave is greater than that of S wave velocity, indicating that the major contribution comes from the face-parallel cracks. No obvious pattern was observed for Coconino sandstone.

Although we can determine the elastic wave velocity from a given crack distribution, the converse is not true. It is impossible to determine the exact crack distribution in rocks just from elastic wave velocity measurements since the distribution of cracks is not a unique function of the velocities (Nur 1971). Further experiments are under way to study the different contributions to velocity reductions of different oriented cracks.

Interpretation of V_p/V_s

Since shear wave velocity is less sensitive than the compressional wave velocity to the presence of cracks normal to the propagation direction of the wave (Nur 1971; Anderson et al. 1974), we can use V_p/V_s to characterize the orientation of cracks for the 3 types of rocks. The average pre-shot V_p/V_s is ~1.9 for San Marcos gabbro (Fig. 5a) and ~1.7 for Sesia eclogite (Fig. 5b). The post-shot V_p/V_s for both types of rocks are less than the pre-shot value, indicating the cracks produced by the shock were mainly oriented parallel to the impact surfaces. The post-shot V_p/V_s for both types of rocks decrease with increasing computed tensile stress, which means higher crack density. No good reason exists for the random pattern of post-shot V_p/V_s for Coconino sandstone (Figs. 5c and 5d). Further work should be conducted to study the anisotropy of sandstone.

Strain-Rate Effect

It has long been recognized in fracture mechanics that material strength depends on the rate at which the loading is applied. Dynamic tensile strength of rocks at high strain rates produced by shock wave interactions can exceed the quasi-static tensile strength by an order of magnitude (Grady and Hollenbach 1979). Cohn and Ahrens (1981) came to a similar conclusion in their studies of analogues of lunar rocks. Similar behavior has been observed for ice-silicate mixtures (Lange and Ahrens 1983). Grady and Lipkin (1980) have generalized a wide range of data suggesting dependence of tensile fracture strength on strain rate. Grady (1998) gives the

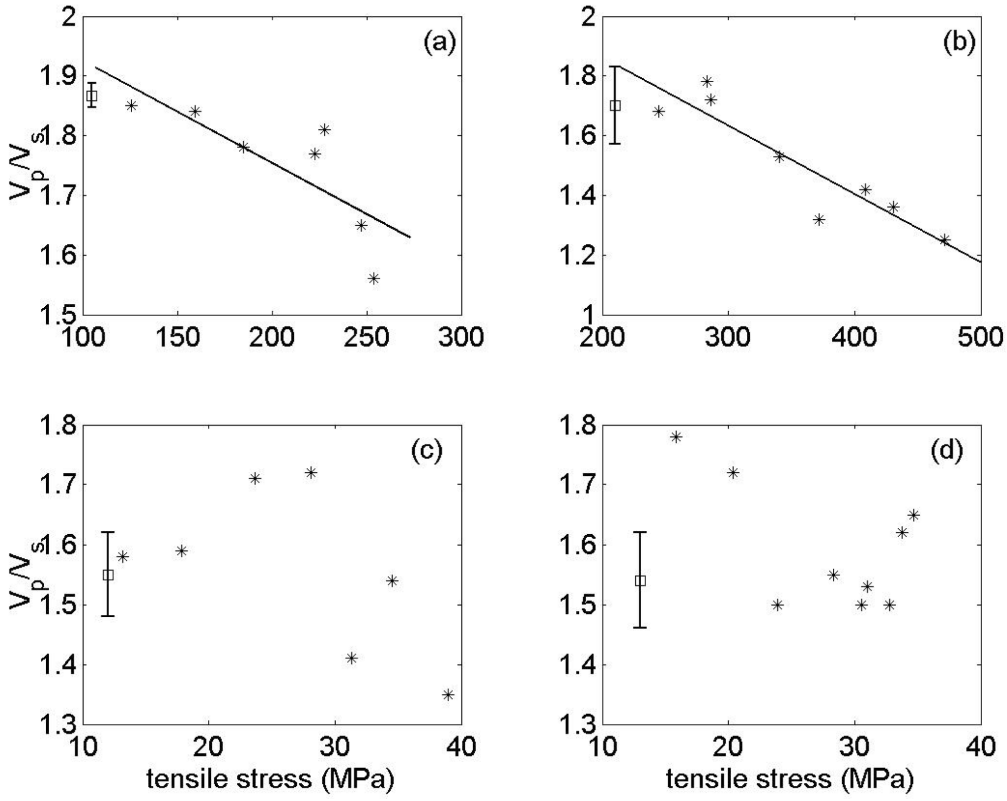

Fig. 5. Post-shot V_p/V_s values versus computed tensile stress: a) San Marcos gabbro; b) Sesia eclogite; c) Coconino sandstone with a 2.4 μs duration time; d) Coconino sandstone with a 1.4 μs duration time. The open squares are average pre-shot V_p/V_s: 1.87 for San Marcos gabbro, 1.7 for Sesia eclogite, and 1.54 for Coconino sandstone. The error bars represent the lower and upper limits of the pre-shot V_p/V_s value. The stars are post-shot V_p/V_s values. The straight lines in (a) and (b) are linear fit of the post-shot results for San Marcos gabbro and Sesia eclogite. The post-shot V_p/V_s decreases with computed tensile stress for both cases. The post-shot V_p/V_s values of Coconino sandstone for the 2 duration time cases are scattered. No obvious relation between the post-shot V_p/V_s and the tensile stress is observed for Coconino sandstone.

strain rate-dependent criteria of tensile strength (σ_t) for ceramics:

$$\sigma_t = (6\rho^2 c^3 \dot{\varepsilon})^{1/3} \quad (7)$$

where c is the compressional wave velocity, ρ is the density and $\dot{\varepsilon}$ is the strain rate, defined as:

$$\dot{\varepsilon} = \frac{\varepsilon}{\Delta t} \quad (8)$$

ε is strain, and Δt is the duration time. Lange et al. (1983) give ε as a function of known material parameters:

$$\varepsilon = \frac{\rho_i V_i}{\rho_i V_i + \rho_t V_t} \frac{U_p}{V_t} \quad (9)$$

Generally, the tensile strength is proportional to a power of the strain rate, with the power law exponent typically around 1/4 to 1/3, depending on the materials (Grady and Lipkin 1980; Housen and Holsapple 1990; Grady 1998).

The porous Coconino sandstone is expected to behave differently from ceramics. However, the assumption is still valid that the dynamic tensile strength is proportional to a power of the strain rate. Taking our experiment results of 20 MPa at a 1.4 μs duration time and 17 MPa at a 2.4 μs duration time, the power law exponent is calculated to be 1/3.3 for Coconino sandstone. The strain, ε, is assumed to be the same for the 2 duration time experiments. The power law exponent fits very well within the range of the previous study, 1/4 to 1/3 (Grady and Lipkin 1980).

The tensile strengths of ice and different rocks at different strain rates are given in Table 3. Also included is σ_c, the tensile strength at a strain rate of 10^6 s^{-1}, extrapolated from available data or measured directly. The dynamic tensile strengths of Coconino sandstone, normalized by σ_c, versus strain rate are plotted in Fig. 6. Also included in Fig. 6 are the

Table 3. Tensile strengths (in MPa) of ice and rocks at different strain rates.[a]

	Strain rate (10^6 s^{-1})							
	10^{-6}	2×10^{-2}	1/2.4	1/1.4	1/1.3	1	1/0.5	σ_c[b]
Coconino sandstone	–	–	17 (1)	20 (1)	–	–	–	–
Donzdonfer sandstone	3 (2)	–	–	–	–	–	–	22[c]
Bedford limestone	–	–	–	–	35 (3)	–	60 (3)	40[c]
Ice	1.6 (4)	17 (4)	–	–	–	–	–	40[c]
San Marcos gabbro	–	–	–	–	–	150 (1)	–	150[d]

[a]Sources: (1) This study; (2) Hajpal and Torok 1998; (3) Ahrens and Rubin 1993; (4) Lange et al. 1984.
[b]Dynamic tensile strength at strain rate of 10^6 s^{-1}.
[c]Extrapolated from available data.
[d]Measured.

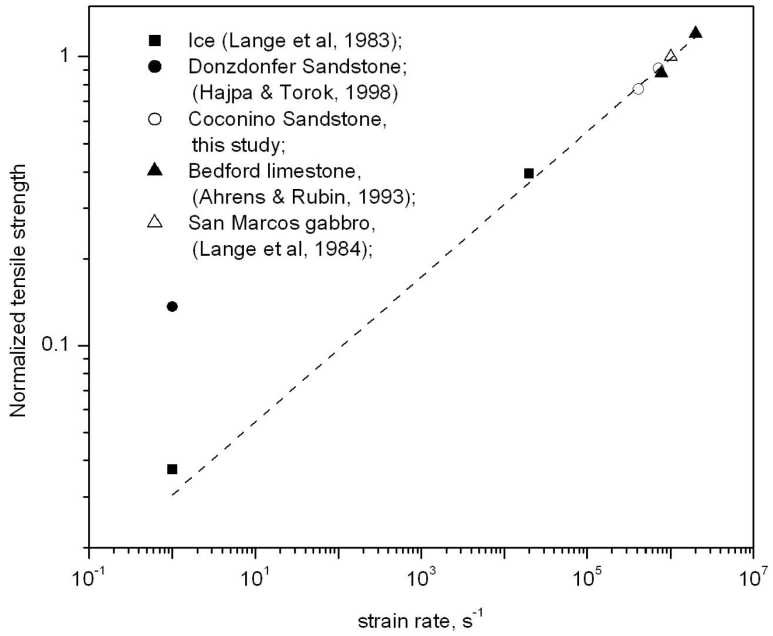

Fig. 6. Normalized tensile strengths as a function of strain rate for ice and rocks. The dash line is a non-linear square fit of $\sigma/\sigma_c = a\dot{\varepsilon}^{1/b}$ to the available data. Note the log scale here. See text for a detailed explanation.

static tensile strength of Donzdonfer sandstone (Hajpal and Torok 1998) and the dynamic ice and Bedford limestone data from previous work (Lange et al. 1983; Ahrens and Rubin 1993). Non-linear square fit for all these data by the relation of $\sigma/\sigma_c = a\dot{\varepsilon}^{1/b}$ gives a = 0.03 ± 0.02 and b = 3.97 ± 0.05.

The tensile strength has a strong dependence on strain rate in the high strain rate region. Care must be taken when applying the experimental measurement of sandstone to field impact craters, for which the strain rate is about 3 orders of magnitude lower, or the duration time is about 3 orders of magnitude longer, than that in the experiments.

APPLICATION TO IMPACT CRATERING

Shock-induced fractures and crack-induced compressional velocity reduction in rocks beneath impact craters have been described by seismic refraction study of craters in the field (Ackermann et al. 1975) and small-scale impact cratering experiments in the laboratory (Polanskey and Ahrens 1990; Ahrens and Rubin 1993; Xia and Ahrens 2001). According to the experiments of Polanskey and Ahrens (1990), 4 types of fractures, concentric, radial, near-surface (spall), and conical, are usually produced beneath impact craters (Fig. 7). The formation and propagation of conical fractures beneath impact craters has also been modeled by computational simulation (O'Keefe et al. 2001).

The peak shock pressure beneath the impact crater displays 3 regimes (Ahrens and O'Keefe 1987) (Fig. 8). The responses of different regions in the target are affected in different ways by the combined effect of dynamic stresses, material strength, and gravity when a shock wave is produced by a large impact. Regime 1 is the impedance match regime, extending to a few projectile radii into the target, where the peak shock pressure is roughly given by the planar impedance match pressure. For hypervelocity planetary impacts, the target material in this region is partially or completely melted. This is the shock melted material that remains in terrestrial craters for craters >10 km in radius.

Regime 2 is the pressure decay regime, which extends to the distance where the pressure equals the Hugoniot elastic

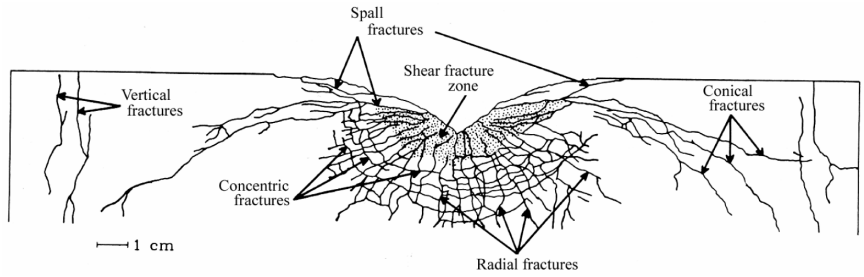

Fig. 7. Cross-section of laboratory impact crater in San Marcos gabbro, showing the 4 types of crack failure (after Polanskey and Ahrens 1990).

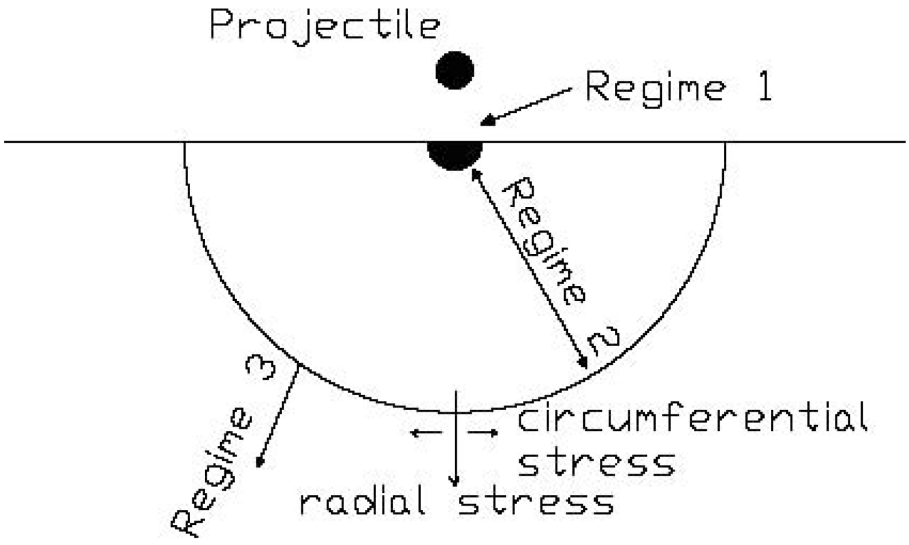

Fig. 8. Three regions of peak shock pressure beneath impact crater. Regime 1 is the impedance match regime, regime 2 is the pressure decay regime, and regime 3 is the elastic decay regime. The radial stress is perpendicular to the shock front. The radial stress is compression and the circumferential stress is tension. See text for detail explanation.

limit (abbreviated hereafter as HEL) of the target. In regime 2, the pressure decay with distance from the impact is generally described by the empirical relation:

$$\sigma_r = \sigma_0(r/r_0)^{-n} \quad (10)$$

where σ_0 is the contact impact pressure calculated from the standard shock-wave impedance-match solution, r_0 is the radius of the projectile, and n is the stress dependent shock pressure attenuation parameter. For non-porous silicate projectile and target, it is defined as (Ahrens and O'Keefe 1987):

$$n \cong -0.625\log_{10}U - 1.25 \quad (11)$$

where U is impact velocity of the projectile ranging from 5 to 45 km/s. This indicates that the peak pressure for high velocity impacts decreases faster with distance from the impact point than that of low impacts, keeping all the other parameters the same.

Pierazzo et al. (1997) investigated the dependence of (n) on various impact-related parameters, material type, impact velocity, projectile size, and angle from the vertical, by carrying out hydrocode simulations of impact for different materials: dunite, granite, aluminum, iron and ice. The initial conditions are 10 to 80 km/s for impact velocity and 0.2 to 10 km for the projectile radius. They find that material type has a small influence on (n), and give a more general formula:

$$n = a + b\log_{10}(U) \quad (12)$$

for all the materials but ice, where $a = -1.84 \pm 0.17$ and $b = 2.61 \pm 0.14$.

In regime 2, the material is intensely compressively failed such that brittle rock becomes fine powder. For 1–10 km planetary craters on earth, the target material in these regimes does not remain in the crater but is ejected and may fall back into the crater. Laboratory craters in rock are too small to retain much of this regime 2 material. At greater distance, shear failure occurs. This is the so called Grady-Kipp region described by Melosh (1989). Concentric cracks and radial cracks form in this region.

Regime 3 is the elastic decay regime. In this region, we apply the results of Shibuya and Nakahara (1968). Shibuya and Nakahara (1968) calculated the stress state of a semi-infinite elastic body subjected to a concentrated impact load using the theory of elasticity. According to their calculation, at the time when the dilatational wave arrives at a considered point, the radial stress, σ_r, which is perpendicular to the shock front, is compression, and the circumferential stress, σ_θ, is tension except for a short time just after the arrival of the dilatational wave. They also concluded that the stress of the wave fronts decreases nearly in proportion to $1/r^2$ with increasing distance from the impact point. The magnitudes of the 2 stresses have the relation (Shibuya and Nakahara 1968):

$$|\sigma_\theta| \approx \frac{1}{3}|\sigma_r| \quad (13)$$

The circumferential stress (σ_θ) would generate radial fractures when it exceeds the tensile strength of the body. Since the tensile strength is much less than the compressive strength for a given material, radial cracks extend further than the concentric cracks.

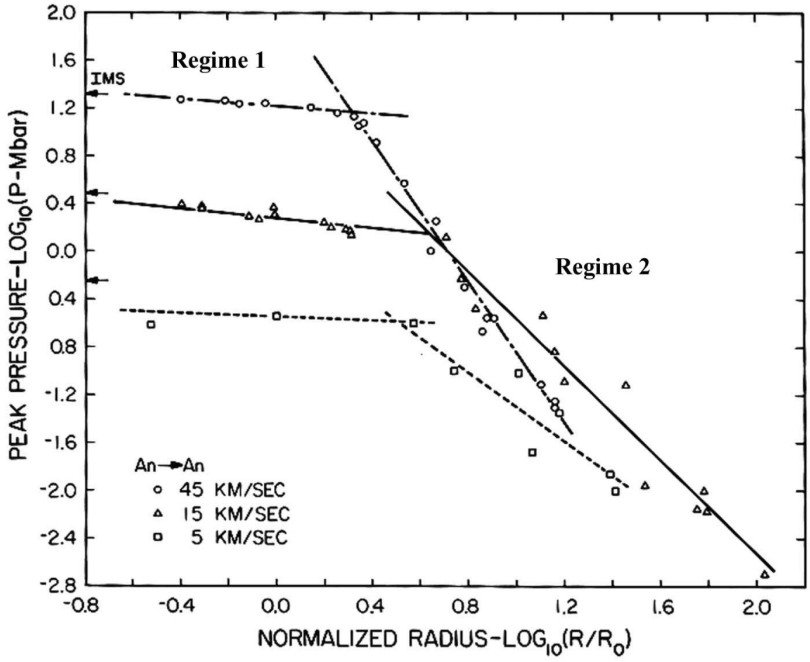

Fig. 9. Peak shock pressure versus normalized radius at various impact velocities for gabbroic anorthosite impactors. The arrows indicate one-dimensional impedance match pressures. Regime 1 and regime 2 are the same as in Fig. 8 (after Ahrens and O'Keefe 1987).

The magnitude of tensile stress versus depth is important to us, since we are concerned with the radial cracks produced by the tensile stress and how far they can propagate. On a planetary scale, gravity effects on tensile failure must also be taken into account when calculating the stress state in rocks beneath the impact in the elastic regime. From the discussion of Shibuya and Nakahara (1968), we take the horizontal tensile stress, σ_θ, as $0.33*\sigma_r$, where σ_r is the radial stress calculated from Equations 10 and 12 from this paper. The radial cracks extend to distances from the impact where σ_θ exceeds the sum of critical dynamic tensile strength of the target (P_c) and the overburden pressure (P_h). Taking tension as positive, the condition for radial cracks to occur at a certain depth (h) is:

$$\sigma_\theta \geq P_c + P_h \tag{14}$$

where P_h equals ρgh, ρ is the density of the overlying rocks, and g is the Earth gravity.

Assuming a point source similarity solution, Holsapple (1993) gives estimates of crater volume for a variety of geological materials. For soft rock material, crater volume, V, is given by (Holsapple 1993):

$$V = 0.009 m U^{1.65} \tag{15a}$$

in the strength regime, where m is the projectile mass (in kg), and U is impact velocity (in km/s). In the gravity regime, it is given by:

$$V = 0.48 m^{0.783} G^{-0.65} U^{1.3} \tag{15b}$$

where G is Earth's gravity, and V is in m^3.

It is important to point out that any observable in the far field, such as damage depth, crater size, etc., is determined by a point-source solution (Holsapple 2003), while the calculation of peak pressure and melt volume are not. Since these various observables are based on inconsistent scaling laws, there is some debate in the impact field about whether it is possible to derive the size and velocity of the projectile for a given impact crater site and known projectile material (Holsapple 2003). Nevertheless, we believe it is constructive to attempt to take an empirical approach and attempt to invert the above information to derive the size and velocity of the projectile separately.

We will apply our present experimental result for Coconino sandstone, combined with other reported parameters (crater volume and density of the projectile) for Meteor Crater, Arizona, to make estimates of the size and velocity of the projectile. Meteor Crater was formed about 50,000 years ago by the impact of an iron meteorite (Shoemaker 1963). The observed volume of the crater is 7.6×10^7 m^3 (Shoemaker 1963). Coconino sandstone is one of the main sedimentary units underlying the Meteor Crater. Seismic refraction investigations of Meteor Crater indicate that the damage depth of the crater is ~850 m (Ackermann et al. 1975).

We infer below that the characteristic projectile dimension for Meteor Crater is 10 to 10^2 m. As this compares to 10^{-3} m for the characteristic dimension of our flyer plate, the time scales of tensile loading the rocks beneath Meteor Crater are 10^3 to 10^4 longer. Taking the strain rate of impact that produced Meteor Crater as 5×10^3 s^{-1}, the extrapolated dynamic tensile strength of Coconino sandstone at this strain rate is ~7 MPa from Fig. 6 and the previous discussion. Because of the deficit of experimental data of dynamic tensile strength for sandstone, this is just a rough estimation.

Combinations of impact velocities, U (km/s), and impactor radii, a_0 (m), are constrained by the damage depth of Meteor Crater, the tensile strength of target material (Coconino sandstone), and the volume of the crater. There is a discrepancy about whether Meteor Crater is in the strength regime or gravity regime. According to the criteria of Holsapple (1993), Meteor Crater is within the gravity regime. However, according to the definition of Ahrens et al. (2002), Meteor Crater, with a diameter of about 1 km, is within the strength regime in the damage depth versus crater diameter space. We use both equations to calculate the volume of Meteor Crater. Our calculations find that in the strength regime, an impact with U = 33 km/s, a_0 = 9 m satisfies parameters of an iron impactor density, damage depth, and dynamic tensile strength, as well as an observed volume of Meteor Crater. If the crater is gravity-dominated, a combination of U = 41 km/s, a_0 = 12 m satisfies all the required parameters. The kinetic energy of this projectile, expressed in Mton of TNT is given as:

$$E_k = \frac{1}{2} m U^2 / (4.18 \times 10^{15}\ \mathrm{J/Mton}) \tag{16}$$

For the first case, E_k is 3.12 Mt and is 11.42 Mt for the second case. The first result agrees with the estimate of Polanskey and Ahrens (1994) of 2.4 to 8.9 Mt and is close to the 3.8 Mt used by Roddy et al. (1980) in their simulations of the formation of Meteor Crater. We prefer the strength regime solution of 33 km/s as a more plausible asteroid impact velocity on Earth (although quite higher than typical values for asteroidal impacts on Earth). The stress versus depth (normalized by the radius of the projectile) of the strength regime impact is shown in Fig. 10.

CONCLUSION

Three types of terrestrial rocks, San Marcos gabbro, Coconino sandstone, and Sesia eclogite, were subject to planar impacts to produce tensile failure under dynamic loading conditions. Two sets of experiments with different duration times were conducted for porous sandstone. Ultrasonic velocity measurements of pre-shot and post-shot samples were measured to determine the dynamic tensile strength and the fracture strength of each type of rock by detectable velocity reduction. The major results are:

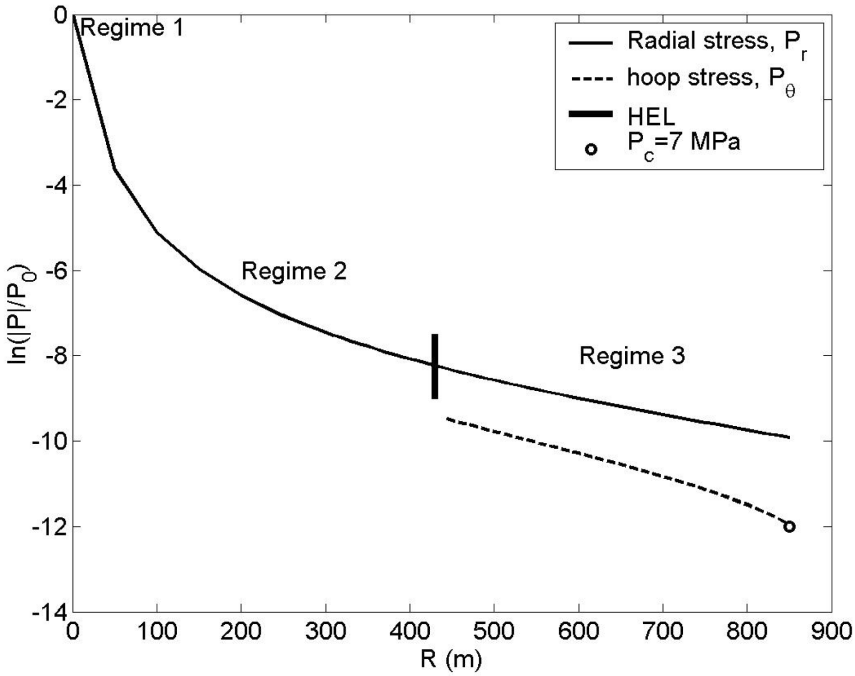

Fig. 10. Normalized amplitudes of stress, P, at different depths, R, for impact with velocity U = 33 km/s, and impactor radius r_0 = 9 m. The impact is constrained by damage depth of Meteor Crater (850 m), crater volume, V = 7.6e7 m^3, and dynamic tensile strength of Coconino sandstone, P_c = 7 MPa (see text for explanation). The solid line is radial stress, the dashed line is circumferential tensile stress. The heavy line is where the Hugoniot elastic limit (~300 MPa) is reached. The circle is where the depth is 850 m and the peak circumferential tensile stress, 7 MPa, occurs.

1. The onset of cracking occurs at ~150 MPa for San Marcos gabbro, ~20 MPa for Coconino sandstone for the 1.4 μs duration time case, and ~17 MPa for the 2.4 μs duration time case, and ≤240 MPa for Sesia eclogite. Complete fracture occurs above 250 MPa for gabbro, 40 MPa for sandstone, and ~480 MPa for eclogite.
2. Both reductions of P and S wave reduction for all 3 types of rocks increase with the computed tensile stress, indicating that the higher tensile pressure produced higher crack density. V_p/V_s of post-shot San Marcos gabbro and Sesia eclogite samples decrease with the computed tensile pressure. No obvious relation between post-shot V_p/V_s of Coconino sandstone and the computed tensile pressure is observed.
3. Higher reduction of P wave than S wave velocity in both San Marcos gabbro and Sesia eclogite indicates that spall (subparallel to the impact surface) cracks contribute more to the velocity reduction than radial cracks. The random pattern of reductions of P and S wave velocity for Coconino sandstone is possibly caused by its high porosity and variety between separate samples. V_p/V_s of post-shot San Marcos gabbro and Sesia eclogite samples are less than the pre-shot values.
4. Shock-induced fracture in rocks and the seismic velocity reduction caused by the fracture are some of the major characteristics of impact craters. The damage depth of the impact crater is controlled by the equation-of-state of projectile and target and by the impact velocity and dimension of the projectile. Assuming other parameters are known, we use the impactor density and fracture depth (850 m) for Meteor Crater, Arizona and the dynamic tensile strength of Coconino sandstone extrapolated from our experiments (7 MPa) to obtain some rough estimates of impact velocity U (km/s) and impactor radius, a_0 (m), combinations. Taking into account parameters of volume of the crater, an impact with U = 33 km/s, a_0 = 9 m is derived assuming that Meteor Crater is strength-dominated. If gravity scaling is assumed, our solution yields U = 41 km/s, a_0 = 12 m. Because the strength scaled solution yields an impact velocity (33 km/s) closer to the average impact velocity of asteroid impactor on the Earth (20 km/s), and the impact energy of 3.12 Mtons agrees closely with a previous study of Meteor Crater, we prefer the strength-dominated solution.

Acknowledgments–Research supported by NASA. We appreciate the technical support of E. Gelle, M. Long, and the advice of Professor G. Ravichandran. The paper benefited from the helpful comments of Kevin Housen and E. Pierazzo. Contribution #8942. Division of Geological and Planetary Sciences, Caltech.

Editorial Handling—Dr. E. Pierazzo and Dr. R. Herrick

REFERENCES

Ackermann H. D., Godson R. H., and Watkins J. S. 1975. A seismic refraction technique used for subsurface investigations at Meteor Crater, Arizona. *Journal of Geophysical Research* 80: 765–775.

Ahrens T. J. and Rubin A. M. 1993. Impact-induced tensional failure in rock. *Journal of Geophysical Research* 98:1185–1203.

Ahrens T. J. and Gregson, Jr. V. G. 1964. Shock compression of crustal rocks; Data for quartz, calcite, and plagioclase rocks. *Journal of Geophysical Research* 69:4839–4874.

Ahrens T. J. and O'Keefe J. D. 1987. Impact on the earth, ocean, and atmosphere. *International Journal of Impact Engineering* 5:13–32.

Ahrens T. J., Xia K., and Coker D. 2002. Depth of cracking beneath impact craters: New constraint for impact velocity. In *Shock-compression of condensed matter,* edited by Furnish M. D., Thadhani N. N., and Horie Y. New York: American Institute of Physics. pp. 1393–1396.

Anderson D. L., Minster B., and Cole D. 1974. The effect of oriented cracks on seismic velocities. *Journal of Geophysical Research* 79:4011–4015.

Birch F. 1960. The velocity of compression waves in rocks to 10 kilobars, 1. *Journal of Geophysical Research* 65:1083–1102.

Carter W. J. 1978. Explosively produced fracture of oil shale. Progress Report LA-7357-PR. Los Alamos: Los Alamos National Laboratory.

Cohn S. N. and Ahrens T. J. 1981. Dynamic tensile strength of lunar rock types. *Journal of Geophysical Research* 86:1794–1802.

Grady D. E. 1998. Shock-wave compression of brittle solids. *Mechanics of Materials* 29:181–203.

Grady D. E. and Lipkin L. 1980. Criteria for impulsive rock fracture. *Geophysical Research Letters* 7:255–258.

Grady D. E. and Hollenbach R. E. 1979. Dynamic fracture strength of rock. *Geophysical Research Letters* 6:73–76.

Hajpal M. and Torok A. 1998. Petrophysical and mineralogical studies of Burnt sandstones. 2nd International Ph.D. Symposium in Civil Engineering.

Heinrich K. 1991. *Ultrasonics fundamentals and applications.* New York: Elsevier Science Publishers Ltd.

Holsapple K. A. 1993. The scaling of impact processes in planetary sciences. *Annual Review of Earth and Planetary Sciences* 21: 333–373.

Holsapple K. A. 2003. Does melt volume give the signature of the impactor? Workshop of "Impact cratering: Bridging the gap between modeling and observations." LPI Contribution No. 1155. p. 33.

Housen K. R. and Holsapple K. A. 1990. On the fragmentation of asteroids and planetary satellites. *Icarus* 84:226–253.

King M. S. 2002. Elastic wave propagation in and permeability for rocks with multiple parallel fractures. *International Journal of Rock Mechanics and Mining Science* 39:1033–1043.

Lange M. A. and Ahrens T. J. 1983. The dynamic tensile strength of ice and ice-silicate mixtures. *Journal of Geophysical Research* 88:1197–1208.

Lange M. A., Ahrens T. J., and Boslough M. B. 1984. Impact-cratering and spall fracture of gabbro. *Icarus* 58:383–395.

Matsui T. and Mizutani H. 1977. Why is a minor planet minor. *Nature* 270:506–507.

McQueen R. G., Marsh S. P., and Fritz J. N. 1967. Hugoniot equation of state of twelve rocks. *Journal of Geophysical Research* 72: 4999–5036.

Melosh H. J. 1989. *Impact cratering, Ageological process.* New York: Oxford University Press.

Murri W. J., Young C., Shockey D. A., Tokheim R. E., and Curran D. R. 1977. Determination of dynamic fracture parameters for oil shale, final report to Sandia Laboratories. Report PYD-5046. Stanford Research Institute.

Nishizawa O. 1982. Seismic velocity anisotropy in a medium containing oriented cracks-transversely isotropic case. *Journal of Physics of the Earth* 30:331–347.

Nur A. 1971. Effects of stress on velocity anisotropy in rocks with cracks. *Journal of Geophysical Research* 76:2022–2034.

O'Connell R. J. and Budiansky B. 1974. Seismic velocities in dry and saturated cracked solids. *Journal of Geophysical Research* 79: 5412–5426.

O'Keefe J. D. and Ahrens T. J. 1976. Impact ejecta on the Moon. Proceedings, 7th Lunar and Planetary Science Conference. pp. 3007–3025.

O'Keefe J. D., Stewart S. T., Lainhart M. E., and Ahrens T. J. 2001. Damage and rock-volatile mixture effects on impact crater formation. *International Journal of Impact Engineering* 26:543–553.

Pierazzo E., Vickery A. M., and Melosh H. J. 1997. A reevaluation of impact melt production. *Icarus* 127:408–423.

Polanskey C. and Ahrens T. J. 1990. Impact spallation experiements: Fracture patterns and spall velocities. *Icarus* 87:140–155.

Polanskey C. and Ahrens T. J. 1994. Scaling craters in carbonates: Electron paramagnetic resonance analysis of shock damage. *Journal of Geophysical Research* 99:5621–5638.

Roddy D. J., Schuster S. H., Kreyenhagen K. N., and Orphal D. L. 1980. Computer code simulations of the formation of Meteor Crater, Arizona: Calculations MC-1 and MC-2. Proceedings, 11th Lunar and Planetary Science Conference. pp. 2275–2308.

Shibuya T. and Nakahara I. 1968. The semi-infinite body subjected to a concentrated impact load on the surface. *Bulletin of the Japan Society of Mechanical Engineers* 11:983–992.

Shipman F. H., Gregson V. G., and Jones A. 1971. A shock wave study of Coconino Sandstone. NASA Report CR-1842.

Shoemaker E. M. 1963. Impact mechanics at Meteor Crater, Arizona. In *The solar system, vol. 4.* Chicago: University of Chicago Press. pp. 301–336.

Xia K. and Ahrens T. J. 2001. Impact induced damage beneath craters. *Geophysical Research Letters* 28:3525–3527.

Zimmerman R. W. and King M. S. 1985. Propagation of acoustic waves through cracks rock. In *Rock masses,* edited by Ashworth E. and Balkema A. A. Boston. pp. 739–745.